CONFERENCE PRE-PRINT

HIERARCHY OF TURBULENT TRANSPORT MODELS WITH THE SOLEDGE3X CODE

H. BUFFERAND CEA, IRFM Saint-Paul-Lez-Durance, France Email: hugo.bufferand@cea.fr

M. CAPASSO, G. CIRAOLO, H. CORVOYSIER, J. DENIS, N. FEDORCZAK, Ph. GHENDRIH, E. HAVLICKOVA, D. OLIVEIRA, N. RIVALS, S. SURESHKUMAR, P. TAMAIN, N. VARADARAJAN CEA, IRFM

Saint-Paul-Lez-Durance, France

Y. MARANDET

Aix-Marseille Université, CNRS, PIIM Marseille, France

R. DULL, I. KUDASHEV, F. SCHWANDER, E. SERRE, H. YANG Aix-Marseille Université, CNRS, Centrale Marseille, M2P2 Marseille, France

TCV Team

Swiss Plasma Centre - See author list of H. Reimerdes et al 2022 Nucl. Fusion 62 042018 (https://doi.org/10.1088/1741-4326/ac369b)
Lausanne, Switzerland

Abstract

Efficient and fast predictive simulations of turbulent transport in the tokamak edge plasma remain a challenge and are key for preparing the operation and heat exhaust on fusion power plants. In this contribution, we present the application of a hierarchy of models to describe turbulent transport in edge fluid codes from empirical mean-field transport modelling to first principles 3D turbulent simulations. A reduced turbulent model is also presented to improve predictability of mean-field simulations. The three approaches are applied to simulate the same L-mode attached plasma on TCV. The models are compared with each other as well as with experimental measurements.

1. HIERARCHY OF TURBULENCE MODELS FROM MEAN FIELD TO FIRST PRINCIPLES

Accurate modelling of cross-field turbulent transport in the edge plasma of tokamaks remains a significant challenge. Many key experimental features, such as the formation of edge transport barriers, are still difficult to simulate, especially for ITER-sized tokamaks. Predicting the scrape-off layer (SOL) width or the power load imbalance between the inner and outer divertor legs remain an open issue, and yet their characterization is essential to determine the plasma regimes to be developed in future fusion power plants. First-principles modelling of edge plasma turbulence is therefore a key area of research in the fusion community, as it allows to extrapolate from present day experiments to future tokamaks. In the meantime, reliable and fast simulation of turbulent plasma transport in the edge plasma is required for day-to-day experiment interpretation and plasma scenario design for future machine. The main workhorse for this kind of simulation are transport codes relying on mean-field simulations where the turbulent transport is taken into account by effective diffusivities D_{turb} , usually set empirically. If this kind of mean field simulation lack predictability for the turbulent transport, they enable a full integration of the multi-physics character of the edge plasma (neutral recycling, plasma contamination by eroded species from the wall, impurity seeding...). In order to improve the predictability of mean-field simulations for turbulent transport, reduced-models have been proposed to estimate a priori turbulent diffusivities from edge plasma turbulence physics properties. For instance, one type of reduced models introduces an equation for the turbulent kinetic energy k defined as the kinetic energy associated to fluctuations of plasma velocity $k = \frac{1}{2} m_i \langle \tilde{v}^2 \rangle$, the latter being then linked to the turbulent diffusivity D_{turb} . One can cite the following approaches in the literature [1, 2, 3]. The following hierarchy of models ranging from low predictability mean field interpretative simulations

to semi-empirical reduced-turbulence-models mean field simulations to high fidelity first-principles turbulent simulations is somehow reminiscent to the approach followed in the neutral fluid community where a hierarchy of models is used to describe turbulence transport starting with RANS (Reynolds Averaged Navier-Stokes) simulations which are mean field simulations – with or without reduced models for turbulence, to first-principles LES (Large Eddy Simulation) or DNS (Direct Numerical Simulation) turbulent simulations. Table 1 summarizes this comparison between models used in the plasma and those used in the neutral fluid community.

Table 1 Table summarizing hierarchy of models for turbulence description in plasma and neutral fluid communities

Model	Sub-model	Plasma Community	Neutral Fluid Community		
Mean Field Simulation	Emminical	Interpretative	Reynolds Averaged Navier		
	Empirical	Transport simulations	Stokes (RANS)		
		Transport simulations	RANS with $k - \varepsilon$, $k - \omega$,		
	Reduced-model	with $k, k - \varepsilon, k - \zeta$	Sparlart-Allmaras, Reynolds		
		model	stress models		
First-Principles Turbulent simulations	Large-scales only	- Dl 1. 1	Large Eddy Simulation (LES)		
	All scales	Plasma turbulent simulations	Direct Numerical Simulation		
		simulations	(DNS)		

The SOLEDGE3X fluid code incorporates a broad range of models mentioned above with varying fidelity [4], which allows a stage approach analysis to the problem of edge turbulence. In this contribution, we apply this hierarchy of models to the TCV-X21 experiment carried out at the Swiss Plasma Centre in 2021 which aims at providing the most favourable plasma conditions for confrontation between experimental measurements and turbulence simulations in attached L-mode conditions.

2. IMPLEMENTATION IN THE SOLEDGE3X CODE

The SOLEDGE3X edge plasma fluid code implements Braginskii like equations for multi-component plasmas. The equations are solved in the drift-fluid approximation. The collisional closure for friction forces, viscous terms and heat fluxes relies mostly on Zhdanov closure [5] for non-trace impurities or on simplified algebraic expressions for trace impurities found in [6]. The code can be used as a 2D transport code with prescribed turbulent diffusivities (typically $D_{\perp} \sim 1m^2 s^{-1}$). It can also be used as a 3D turbulence code by setting cross-field diffusivities to classical level (typically $D_{\perp} \sim 10^{-2} m^2 s^{-1}$) and by numerically resolving small scale turbulent structures, thus requiring a sufficiently fine mesh grid.

2.1. Electrostatic and electromagnetic models

The SOLEDGE3X simulations can be run in an electrostatic approximation where the magnetic field is stationary – in that case, the turbulent transport is driven by the interplay between the fluctuations of the electrostatic potential ϕ and those of the density and temperature fields. The edge turbulence is then primarily driven by driftwave and interchange instabilities. Equation (1) recalls the current balance solved in SOLEDGE3X which evolves the electrostatic potential thru a so-called vorticity equation,

$$\frac{\partial}{\partial t} \left(\vec{\nabla} \cdot \left(\frac{m_i}{B^2} \left(n \vec{\nabla}_{\perp} \phi + \frac{1}{Z} \vec{\nabla}_{\perp} p_i \right) \right) \right) = \vec{\nabla} \cdot \left(j_{\parallel} \vec{b} + \vec{j}^{\star} \right) \tag{1}$$

where the parallel current is given by generalized Ohm's law obtained from electron parallel momentum balance:

$$j_{\parallel} = \sigma_{\parallel} \left(-\nabla_{\parallel} \phi + \frac{\nabla_{\parallel} p_e}{n} + 0.71 \nabla_{\parallel} T_e \right) \tag{2}$$

However, even for low β plasmas, fluctuations of the magnetic potential may play a significant role in turbulent transport, especially when strong gradients build up. To capture this effect, SOLEDGE3X now also implements a reduced MHD model where fluctuations of the parallel component of the electromagnetic vector potential are taken into account. In this model, the parallel current is given by the electron parallel momentum balance equation where one introduces the inductive part of the parallel electric field as well as electron inertia:

$$-\frac{m_e}{e} \left(\partial_t j_{\parallel} + \vec{\nabla} \cdot (j_{\parallel} \vec{v}_e) \right) = en \left(\nabla_{\parallel} \phi + \frac{\partial A_{\parallel}}{\partial t} \right) - \nabla_{\parallel} p_e - 0.71 \nabla_{\parallel} T_e + \frac{nj_{\parallel}}{\sigma_{\parallel}}$$
(3)

The parallel magnetic potential is given by Ampère's equation:

$$\vec{\nabla} \cdot (\vec{\nabla}_{\perp} A_{\parallel}) = -\mu_0 j_{\parallel} \tag{4}$$

Introducing inductive effects modifies the fluctuations of the perpendicular electric field due to the coupling between current balance (Poisson equation) and Ampère's equation. This impacts the cross-field turbulent transport. In addition, fluctuations of A_{\parallel} imply small fluctuations of the magnetic field about equilibrium field (small perturbation of the magnetic equilibrium). This effect referred to as magnetic flutter creates an effective cross-field transport (respective to the magnetic equilibrium) induced by parallel transport along a fluctuating magnetic field. The overall impact of these two effects has been studied in the literature both numerically [7, 8] or theoretically [9, 10].

2.2. Reduced model for turbulent transport

Inspired from $k - \varepsilon$ approaches used in the neutral fluid community, SOLEDGE3X implements a reduced model to predict turbulence intensity and subsequent transport. The model is semi-empirical and rely on computing a fluid equation for the fluid moment k characterizing the kinetic energy of fluctuations. This quantity k is used to evaluate turbulent cross-field diffusivities assuming proportionality between k0 and k1, more precisely k2 k3. The equation for k3 is given by:

$$\partial_t k + \vec{\nabla} \cdot (k \vec{v}_i) = \gamma_I k - \varepsilon \tag{5}$$

where $\gamma_I = c_s \sqrt{\frac{\overline{\forall} B}{B} \cdot \frac{\overline{\forall} p_i}{p_i}}$ is the turbulence linear growth rate inspired by interchange instability growth rate. Turbulence will develop favourably on the low field side where interchange is unstable leading to ballooning of cross-field transport. The second term ε in Equation (5) represents turbulence saturation mechanisms. The expression for ε is computed to force a fix-point solution for Equation (5) compatible with turbulent diffusivities required to recover experimental scaling laws for scrape-off layer width, see Ref. [1, 11]. In that sense, an experimental closure is required to fix the degrees of freedom of the model. For L-mode simulation, we usually use a simplified scaling law for the heat flux width that is $\lambda_q = 4q_{cyl}\rho_L$ where q_{cyl} is the cylindrical safety factor and ρ_L the Larmor radius, leading to the following expression for ε :

$$\varepsilon = \gamma_I \frac{2\pi k^2}{\gamma_e q_{cyl} (4\rho^* A^{-1} c_s)^2}$$

where $\gamma_e = 4.5$ is electron sheath transmission coefficient, $\rho^* = \rho_L/a$ is the normalized Larmor radius, A = R/a is the aspect ratio and c_s is the sound speed.

The k-model can be extended to add a fluid equation for ε . Other models in the community [2] propose another closure for saturation mechanisms based on the enstrophy ζ . Despite being rather crude, the k-model already improves the predictability compared to a pure empirical setting of cross-field diffusivities by both predicting the localisation of cross-field transport (ballooning, turbulence in the divertor...). It also automatically predicts a level of transport compatible with experimental scaling laws, meaning an automatic adjustment of cross-field diffusivities with main operational quantities (toroidal magnetic field, plasma current...). It has been successfully applied to TCV [11], WEST and JET [12] tokamaks.

3. THE TCV-X21 EXPERIMENT BENCHMARK

In order to validate edge turbulence codes, a series of shots have been performed on TCV tokamak at the Swiss Plasma Center in 2021. One of the main difficulties for edge turbulence simulation is to reach the necessary resolution to properly describe the fine, almost field-aligned, turbulent filaments. The typical size of these turbulent structure's scales with the Larmor radius while the typical size of the domain to simulate scales with the size of the machine (given for instance by the minor radius *a*). The number of grid points to mesh a poloidal plane

thus scales with $1/\rho_{\star}^2 = \left(\frac{a}{\rho_L}\right)^2$. Concerning the number of poloidal planes needed to mesh the toroidal direction, the constraint will depend on the numerical method used to treat the parallel direction but in the worst case, the number of points in this third direction will also be proportional to $1/\rho^{\star}$. Hence, to reduce the number of grid points, one must increase ρ^{\star} and thus operate at rather low magnetic field. That is the purpose of the TCV-X21 shots which were performed with a reduced magnetic field, namely $B_t = 0.95T$ compared with the nominal $B_t = 1.4T$ for TCV. Moreover, the shots were low power L-mode Ohmic plasmas since L-mode plasmas are considered simpler to simulate. Finally, the TCV-X21 plasmas were operated at low density to remain as much as possible in the attached low recycling regime where plasma-neutral interaction is less crucial. We summarize in Table 2 below the main parameters of the TCV shot #51333 part of the TCV-X21 database that we use latter in this contribution.

Table 2: Main parameters of TCV #51333, representative of TCV-X21 discharge conditions

Parameter	R	а	$B_{oldsymbol{\phi}}$	I_p	q_{95}	f_{GW}	P_{Ohm}
Value	0.88m	0.25m	0.95 <i>T</i>	165 <i>kA</i>	3.2	0.25	150 <i>kW</i>

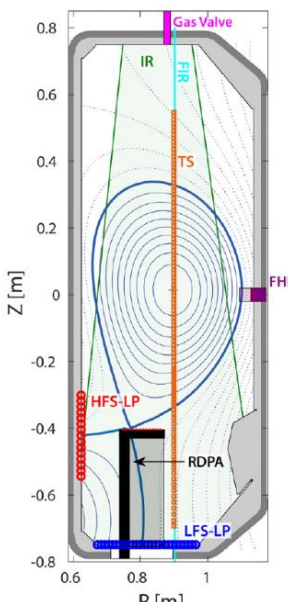


Figure 1 shows Magnetic equilibrium as well as location of diagnostics used in the edge plasma.

Figure 1: TCV-X21 magnetic equilibrium from LIUQE reconstruction. Main diagnostics used fir the edge plasma are shown: Wall embedded Langmuir probes (HFS-LP and LFS-LP), HRP fast horizontal reciprocating Langmuir probe (FHRP), reciprocating divertor probe array (RDPA), Thomson scattering system (TS), far-infrared interferometer (FIR), Infrared camera (IR). Figure reproduced from [13].

Following the experiment, three edge turbulence fluid codes developed in Europe have simulated the TCV-X21 experiment: GBS, GRILLIX and TOKAM3X. The results are discussed and summarized in [13]. Simulations were then performed without neutrals. Recently, the turbulence code HERMES-3 also validated against the TCV-X21 case [14] without neutrals. The TCV-X21 was also simulated with the transport code SOLPS-ITER to investigate in particular the impact of neutrals [15].

4. SIMULATION SET-UPS

R[m] In this contribution, we present SOLEDGE3X simulations performed with different models to treat turbulent cross-field transport. The hierarchy of models range from empirical transport simulation to reduced k-model for mean field modelling and finally first principles 3D turbulence modelling. All simulations include plasma recycling with neutrals being modelled kinetically with the EIRENE code [16] coupled to SOLEDGE3X. For all simulations presented in this contribution, the recycling coefficient of deuterium on the wall is set to a rather low value of R = 90%. Also, a gas puff is used to control plasma density with a feedback loop on the gas puff rate to set separatrix density at $n_{sep} = 7.5 \times 10^{19} m^{-3}$.

4.1. Interpretative mean field modelling

The first set of simulations is run following empirical approach taking directly experimental data to set simulation free parameters. SOLEDGE3X takes as input directly the radial profiles of electron density and temperatures fitted from HRTS midplane measurements, see *Figure 2*. The code automatically adjusts cross-field diffusivities to match the experimental data and gives as an output the radial profiles of particle diffusivity D and electron heat conductivity χ_e (the ion heat conductivity is assumed to be the same, that is $\chi_i = \chi_e$). The diffusivity profiles are shown on *Figure 2*.

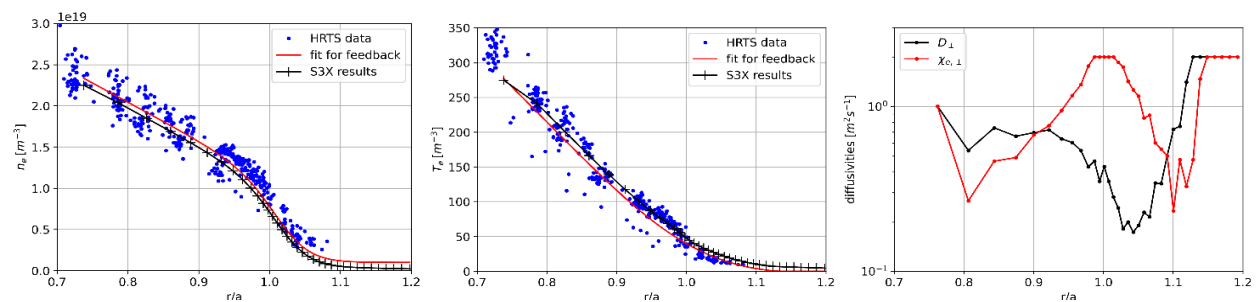


Figure 2: Midplane profiles. Left and center: density and electron temperature profiles showing experimental data (blue symbols) and analytical fit (red) used as an input to SOLEDGE3X simulation. Black lines represent simulation results. Right: cross-field diffusivities computed by SOLEDGE3X to fit experimental profiles.

The simulations are run considering either a pure deuterium plasma or a mixed deuterium-carbon plasma where the carbon is generated by erosion of the wall (the erosion is mostly governed by the chemical sputtering whose yield is set to 2%). The mean-field drifts are not taken into account. The automated procedure to set cross-field

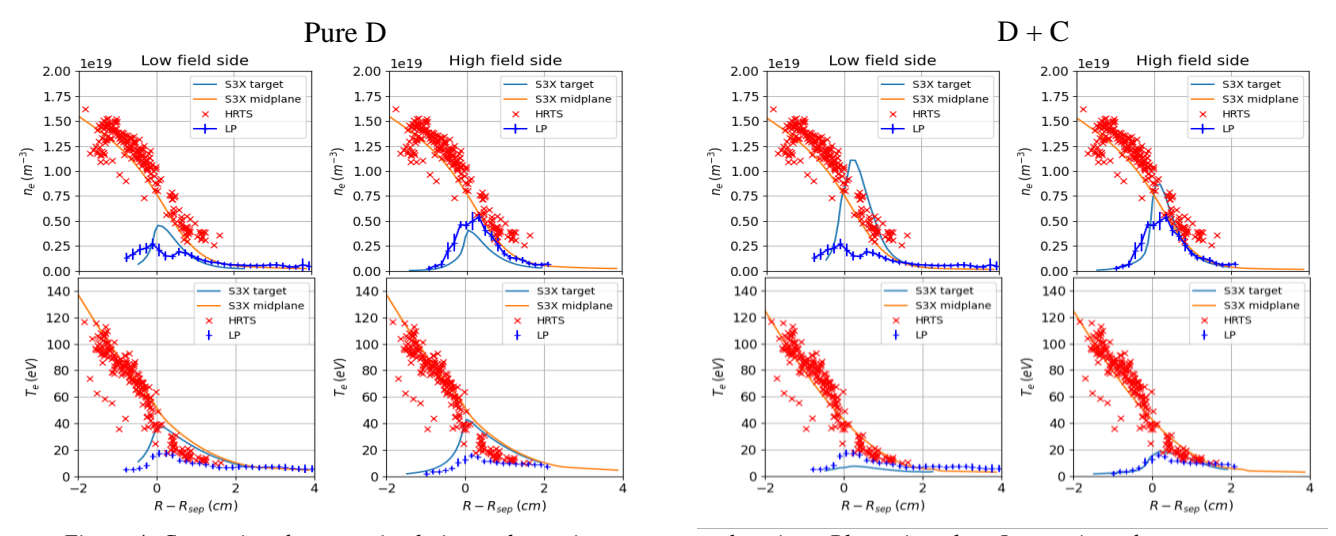


Figure 4: Comparison between simulation and experiments at target locations. Blue points show Langmuir probes measurements while blue lines show simulation data. Midplane data are shown for comparison (HRTS data in red symbols, simulation data in orange line). All data are remapped at the outboard midplane. On the left side are shown simulation results in pure deuterium plasma. On the right side are plotted simulation results including Carbon sputtering.

diffusivities enables an almost perfect match between simulation results and experimental data at the midplane. One now focuses on the divertor region to see if simulation results and experimental data are in good agreement.

Figure 3 shows comparison between simulation results and Langmuir probe data on the wall for the two simulation set-ups (with or without carbon). The carbon case exhibits a lower divertor temperature in better agreement with experimental Figure 4 measurements. shows comparison for parallel heat flux on the LFS target for the two cases. The simulation results are compared with infrared measurements and show again a better agreement for the Carbon case where a significant

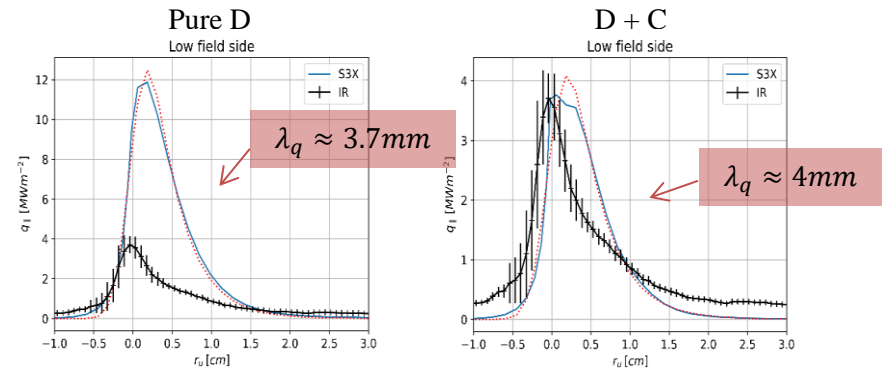


Figure 3: Heat flux on LFS target plates. Black symbols represent IR data, blue lines simulation results and dotted red lines show analytical fit with the function given by Eich in [18].

amount of the power is radiated in the Scrape-off layer reducing the heat flux deposition on the target plates. The heat flux decay length estimated for IR data is found be around 4mm which is recovered by the modelling:

 $\lambda_{q,simu} \sim 4mm$. The typical cost of such a simulation is about 1 day of simulation on 192CPUs. The ability to recover experimental trend is good but there is no predictability since simulations rely on experimental profiles as inputs.

4.2. Reduced-turbulence model for mean-field transport modelling

A similar transport simulation is run with the reduced k-model for turbulent transport estimation. A pure D plasma is considered. This time, the input of the code is the heating power (set to P = 170kW). No further input

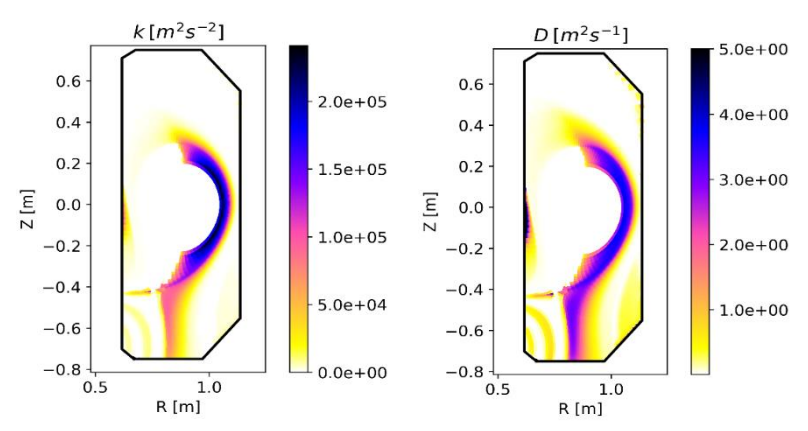


Figure 5: Reduced turbulence model simulation results. Left: kinetic turbulent energy, right: turbulent effective diffusivity.

parameters are needed since cross-field diffusivities are computed by the reduced turbulence model. *Figure 5* shows the turbulent kinetic energy *k* and the cross-field diffusivity predicted by the model. It is localised at the LFS where interchange is unstable.

Comparison between experimental and simulated profiles are shown at midplane and target profiles on *Figure 6*. A rather good agreement is obtained for temperature profiles, especially in the outboard midplane.

The density profiles predicted by the modelling are too flat, leading to an overestimation of the heat flux decay length, as can be shown on *Figure 7* showing heat flux profiles on the LFS target.

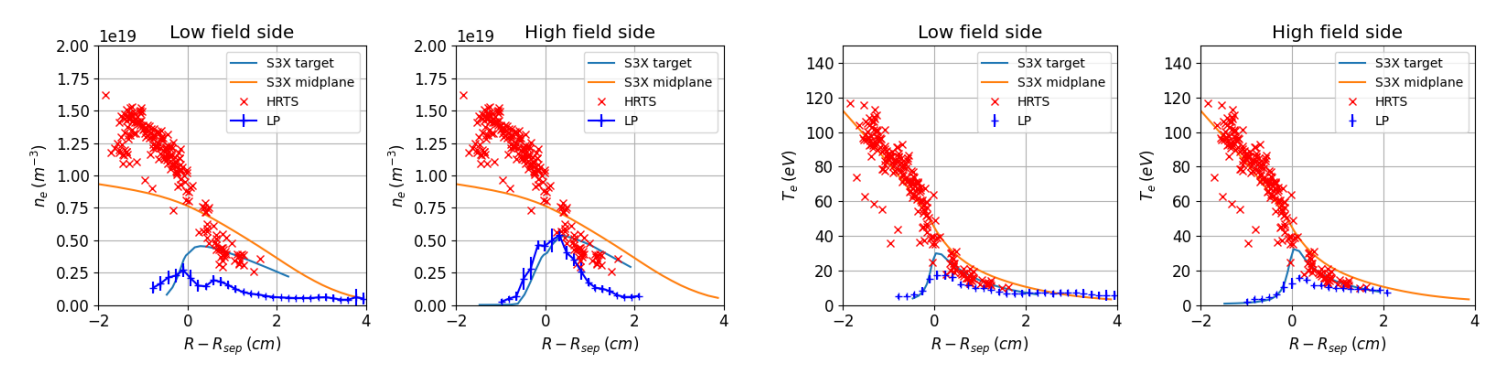


Figure 6: Comparison between experimental and simulated profiles with the k-model. Left: density, right: electron temperature

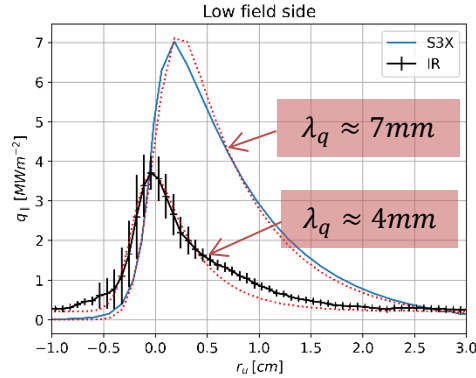


Figure 7: Heat flux on the LFS target. Black symbols: experimental IR measurements. Blue line: simulation results. Red dotted line: analytical fits.

The overestimation of λ_q by the reduced model can be explained by the underlying semi-empirical closure on turbulence saturation. Indeed, the saturation mechanism is adjusted to recover a turbulent transport compatible with a simplified L-mode scaling law for λ_q that is $\lambda_q^{scaling} = 4q_{95}\rho_L$. Assuming $T \approx 30eV$ and with $B_T = 0.95T$ and $q_{95} = 3.2$, the scaling law predicts $\lambda_{q,TCV-X21}^{scaling} = 11mm$ for the TCV-X21 experiment, far from the 4mm measured by the IR diagnostic. The fact that this specific shot does not follow the chosen scaling law shows the limits of this semi-empirical approach. It adds hints of the physics underlying turbulent transport hence improving the predictability of the simulation but remains sensitive to the choices made to close empirically the model. The numerical cost however remains limited to 1 day of computation on 192 CPUs.

4.3. First principles turbulence modelling

Finally, first principles 3D simulation in pure Deuterium were run until reaching a quasi-steady state. The turbulence is purely electrostatic (the fluctuations of the magnetic field are not considered). The input power is

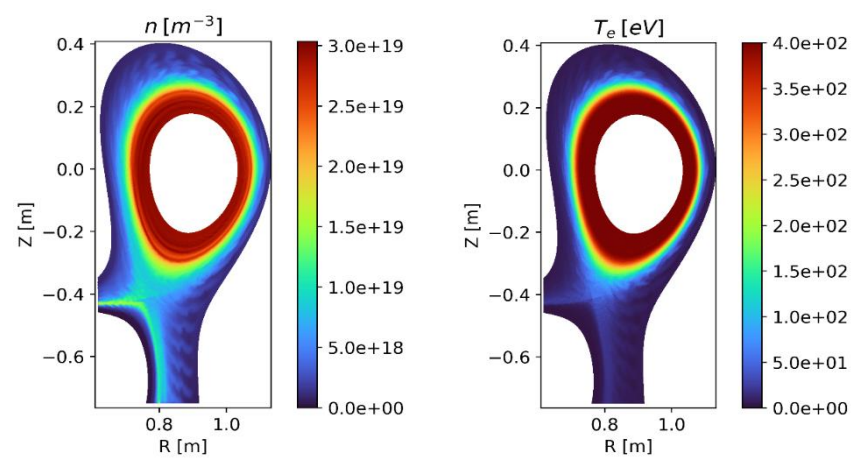


Figure 8: Snapshots of density and electron temperature maps for the TCV-X21 turbulent simulation

set to P = 170kW and the density is controlled by feedback on the gas puff. Figure 8 shows typical simulation results showing turbulent structures propagating in the scrape-off layer. Again, one can plot radial profiles at the outboard midplane and at the target, see Figure 9. One can notice a very good agreement for density and temperature decay length in the scrape-off layer at the outboard midplane, despite a slightly higher temperature value. On the target plates, the temperature is quite well recovered but the density overestimated (simulation results more compatible with a high-

recycling regime). One notices the presence of the two peaks in the density profile at the LFS target, also observed on the Langmuir probes data. *Figure 10* shows heat flux deposition on the LFS target. Simulation results are in

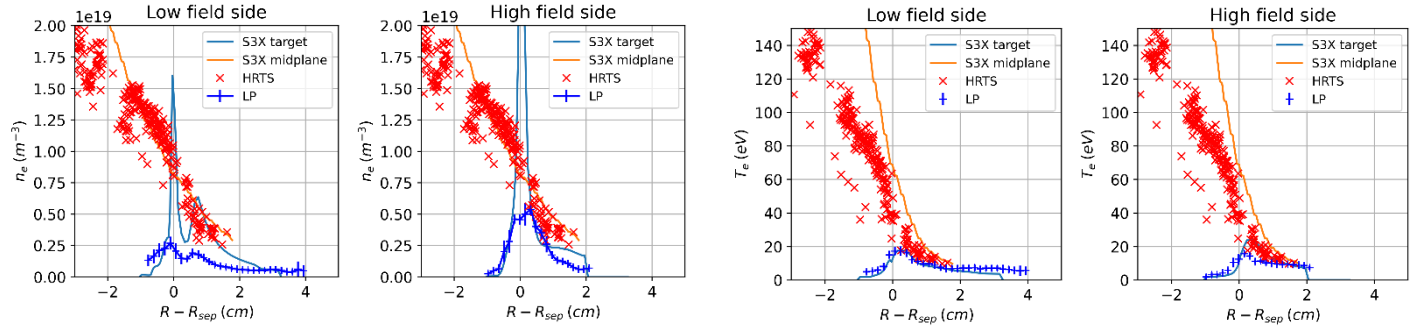


Figure 9: Midplane and target profiles of density and temperature for the turbulent simulation

rather good agreement concerning heat flux width λ_q which is found to be in the range of 4mm. The heat flux is however overestimated in the simulation, probably due to the lack of Carbon in the simulated plasma to radiate and dissipate a significant fraction of the power in the scrape-off layer.

5. CONCLUSIONS

The hierarchy of models to describe turbulent transport has been applied to simulate the TCV-X21 L-mode attached reference plasma scenario. The standard empirical approach used in 2D transport modelling to interpret experiment is found to be very effective to reproduce a specific experimental scenario but without any predictive ability. The efficiency to reproduce experimental trend requires implementing neutral recycling but also carbon sputtering and radiation. First-principles 3D turbulent modelling also recover experimental trends, in particular scrape-off layer width λ_q . For a more quantitative agreement between turbulent simulation results experimental measurements, it will be necessary to add carbon sputtering and radiation in the simulation as suggested by the mean-field simulation results. In between these two approaches, the reduced turbulent model is a way to keep investigating and improving to improve mean-field modelling predictability at a

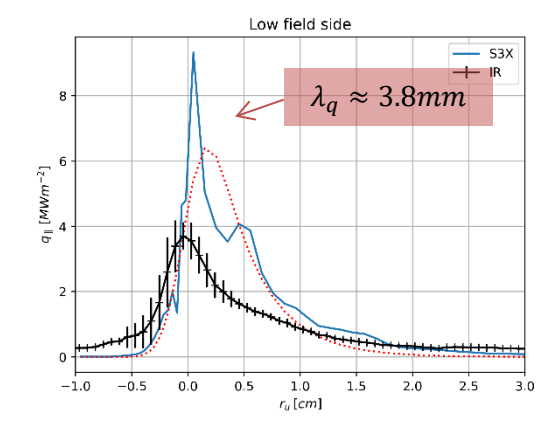


Figure 10: Heat flux on the LFS target. Comparison between experimental IR data (black symbols) and turbulent simulation results (blue line). Red dotted line shows analytical fit to extract λ_a .

lower numerical cost than first-principles turbulent models. When applied to the TCV-X21 case, the current k-model implemented in SOLEDGE3X fails to recover the experimental scrape-off layer width due to the semi-empirical closure used in the model based on λ_q scaling-law (the scaling law overestimating the scrape-off layer width when applied to the TCV-X21 parameters).

ACKNOWLEDGEMENTS

The datasets used in this work are part of DOI's paper and were provided by D. S. Oliveira, D. Galassi, C. Theiler, C. Colandrea, H. de Oliveira, S. Gorno, N. Offeddu, H. Reimerdes, C Wuthrich and TCV team [Coda NF2019]. This project was provided with computing HPC and storage resources by GENCI at CINES and TGCC thanks to the grant 2025-A0180510482 on the supercomputer Joliot Curie's SKL and ROME partitions and on the supercomputer Adastra's GENOA partition. This work has been carried out within the framework of the EUROfusion Consortium, funded by the European Union via the Euratom Research and Training Programme (Grant Agreement No 101052200 — EUROfusion). Views and opinions expressed are however those of the author(s) only and do not necessarily reflect those of the European Union or the European Commission. Neither the European Union nor the European Commission can be held responsible for them.

REFERENCES

- [1] S. Baschetti, H. Bufferand, G. Ciraolo, P. Ghendrih, E. Serre and W. team, "Self-consistent cross-field transport model for core and edge plasma transport," *Nuclear Fusion*, vol. 61, p. 106020, 2021.
- [2] R. Coosemans, W. Dekeyser and M. Baelmans, "A new mean-field plasma edge transport model based on turbulent kinetic energy and enstrophy," *Contrib. Plasma Phys.*, vol. 60, p. e201900156, 2020.
- [3] K. Miki, P. H. Diamond, Ö. D. Gürcan, G. R. Tynan, T. Estrada, L. Schmitz and G. S. Xu, "Spatio-temporal evolution of the L → I → H transition," *Phys. Plasmas*, vol. 19, p. 092306, 2012.
- [4] H. Bufferand, J. Bucalossi, G. Ciraolo, G. Falchetto, A. Gallo, P. Ghendrih, N. Rivals, P. Tamain, H. Yang, G. Giorgiani, F. Schwander, M. S. d'Abusco, E. Serre, Y. Marandet, M. Raghunathan, W. Team and t. J. Team, "Progress in edge plasma turbulence modelling—hierarchy of models from 2D transport application to 3D fluid simulations in realistic tokamak geometry," *Nuclear Fusion*, vol. 61, p. 116052, 2021.
- [5] H. Bufferand, J. Balbin, S. Baschetti, J. Bucalossi, G. Ciraolo, P. Ghendrih, R. Mao, N. Rivals, P. Tamain, H. Yang, G. Giorgiani, F. Schwander, M. S. d'Abusco, E. Serre, J. Denis, Y. Marandet, M. Raghunathan, P. Innocente, D. Galassi and J. Contributors, "Implementation of multi-component Zhdanov closure in SOLEDGE3X," *Plasma Physics and Controlled Fusion*, vol. 64, p. 055001, 2022.
- [6] P. Stangeby, The Plasma Boundary of Magnetic Fusion Devices, London: IoP, 2000.
- [7] R. Düll, .. Bufferand, E. Serre, G. Ciraolo, V. Quadri, N. Rivals and P. Tamain, "Introducing electromagnetic effects in Soledge3X," *Contributions to Plasma Physics*, vol. 64, 2024.
- [8] K. Zhang, W. Zholobenko, A. Stegmeir, K. Eder and F. Jenko, "Magnetic flutter effect on validated edge turbulence simulations," *Nuclear Fusion*, vol. 64, p. 036016, 2024.
- [9] B. D. Dudson, S. L. Newton, J. T. Omotani and J. Birch, "On Ohm's law in reduced plasma fluid models," *Plasma Physics and Controlled Fusion*, vol. 63, p. 125008, 2021.
- [10] B. Scott, "Tokamak edge turbulence: background theory and computation," *Plasma Physics and Controlled Fusion*, vol. 49, pp. S25-S41, 2007.
- [11] S. Baschetti, H. Bufferand, G. Ciraolo, N. Fedorczak, P. Ghendrih, P. Tamain and E. Serre, "A k-epsilon model for plasma anomalous transport in tokamaks: closure via the scaling of the global confinement," *Nuclear Materials and Energy*, vol. 19, pp. 200-204, 2019.

- [12] H. Bufferand, J. Bucalossi, G. Ciraolo, G. Falchetto, A. Gallo, P. Ghendrih, N. Rivals, P. Tamain, H. Yang, G. Giorgiani, F. Schwander, M. S. d'Abusco, E. Serre, Y. Marandet, M. Raghunathan, W. Team and J. Team, "Progress in edge plasma turbulence modelling hierarchy of models from 2D transport application to 3D fluid simulations in realistic tokamak geometry," *Nuclear Fusion*, vol. 61, p. 116052, 2021.
- [13] D. Oliveira, T. Body, D. Galassi, C. Theiler, E. Laribi, P. Tamain, A. Stegmeir, M. Giacomin, W. Zholobenko, P. Ricci, H. Bufferand, J. Boedo, G. Ciraolo, C. Colandrea, D. Coster, H. d. Oliveira, G. Fourestey, S. Gorno, F. Imbeaux, F. Jenko and V. Naulin, "Validation of edge turbulence codes against the TCV-X21 diverted L-mode reference case," *Nuclear Fusion*, vol. 62, p. 096001, 2022.
- [14] B. D. Dudson, M. Kryjak, H. Muhammed and J. Omotani, "Validation of Hermes-3 turbulence simulations against the TCV-X21 diverted L-mode reference case," arXiv preprint (https://arxiv.org/pdf/2506.12180), 2025.
- [15] Y. Wang, C. Colandrea, D. Oliveira, C. Theiler, H. Reimerdes, T. Body, D. Galassi, L. Martinelli, K. Lee and t. T. Team, "Validation of SOLPS-ITER simulations against the TCV-X21 reference case," *Nuclear Fusion*, vol. 64, p. 056040, 2024.
- [16] D. Reiter, M. Baelmans and P. Börner, "THE EIRENE AND B2-EIRENE CODES," *FUSION SCIENCE AND TECHNOLOGY*, vol. 47, pp. 172-186, 2005.
- [17] H. Bufferand, G. Ciraolo, R. Düll, G. Falchetto, N. Fedorczak, Y. Marandet, V. Quadri, M. Raghunathan, N. Rivals, F. Schwander, E. Serre, S. Sureshkumar, P. Tamain and N. Varadarajan, "Global 3D full-scale turbulence simulations of TCV-X21 experiments with SOLEDGE3X," *Nuclear Materials and Energy*, vol. 41, p. 101824, 2024.
- [18] T. Eich, B. Sieglin, A. Scarabosio, W. Fundamenski, R. J. Goldston, A. Herrmann and A. U. Team, "Inter-ELM Power Decay Length for JET and ASDEX Upgrade: Measurement and Comparison with Heuristic Drift-Based Model," *Phys. Rev. Letters*, vol. 107, p. 215001, 2011.